Ground-penetrating Radar Mapping of a Hominid Trackway, Laetoli, Tanzania

Lawrence B. Conyers
Denver, Colorado, USA
lconyers@gpr-archaeology.com
May 19, 2025

Abstract

Very high frequency ground-penetrating radar (GPR) reflection data were collected and processed at Laetoli Site S, to connect an ancient hominid pathway that was uncovered in two excavations conducted in 2016. These footprints have been dated to about 3.6 million years ago and are likely those of Australopithecus afarensis. Profiles were collected 5 cm apart were frequency filtered to enhance specific wave frequencies of interest, and then manually interpreted using 2-D profile analysis. The depth to the prints was digitized and three-dimensional maps were produced, which display the still-buried prints between excavations. Artificial intelligence was used to compare models of the common aspects of 2-D profiles, which defined the known prints, to all the profiles in a portion of the grid. Good spatial correspondence was produced, but the AI map did not produce high quality images of the prints suitable for a detailed print analysis. The comparison of the manually interpreted grid locations with the AI maps showed a greater than 95% spatial correlation, indicating that this method is suitable as a "first round" of data analysis to identify prints' general locations. The two methods should be conducted in unison for future mapping at Laetoli.

Introduction

GPR was conducted at Laetoli July 13-19, 2023 using a GSSI system with paired 2.6 GHz frequency antennas, typically used for concrete evaluation. This GPR equipment transmits radar waves with a wavelength of about 3 cm into the ground to a maximum depth of about 40 cm. Reflections generated from these waves can define objects or features of about 1.5 cm in size or greater, whether they are individual objects of stratigraphic boundaries (Conyers 2023).

Prior to going to the field, a footprint model was produced in the USA and various GPR equipment and collection methods were experimented with to determine what might be possible. That work concluded that antennas with a frequency lower than about 2 GHZ, generating waves longer than about 5-6 cm, would not be capable of imaging prints of the dimensions or depth known from Site S at Laetoli. There the prints have a maximum depth of about 3 cm or so and are buried 10-35 cm below the ground surface (Masao et al. 2016).

All reflection data were collected within a 6-nanosecond time-window with 512 digital samples used to define waves in each trace. Grids grid of profiles were collected with individual profiles 1.5 meters in length spaced 5 cm apart and 4 reflection traces collected every centimeter along transects.

Survey goals and general data analysis to meet those goals

The anticipated outcome of the survey was to measure the depth of the top of the T-7 unit (a volcanic tuff unit #7), which is buried and contains the preserved prints. Two-way radar travel times measured in nanoseconds show that the T-7 unit reflected energy from between 1 and 2 nanoseconds (two-way travel time), which corresponds to a depth of about 20-30 cm.

All GPR antennas transmit radar waves that are both higher and lower in frequency than the stated "center frequency" of the antenna. The 2.6 GHz antenna employed here therefore actually transmitted energy as high as about 5.2 GHz and as low as 1.3 GHz (one octave of the center frequency). To best define the T-7 surface on which the prints were preserved the recorded data were first filtered so that only waves between 2 and 3.5 GHz frequencies were used for display, removing most high and low frequency noise. This retained the recorded waves for display that were best for imaging prints of the expected size and at the depth necessary.

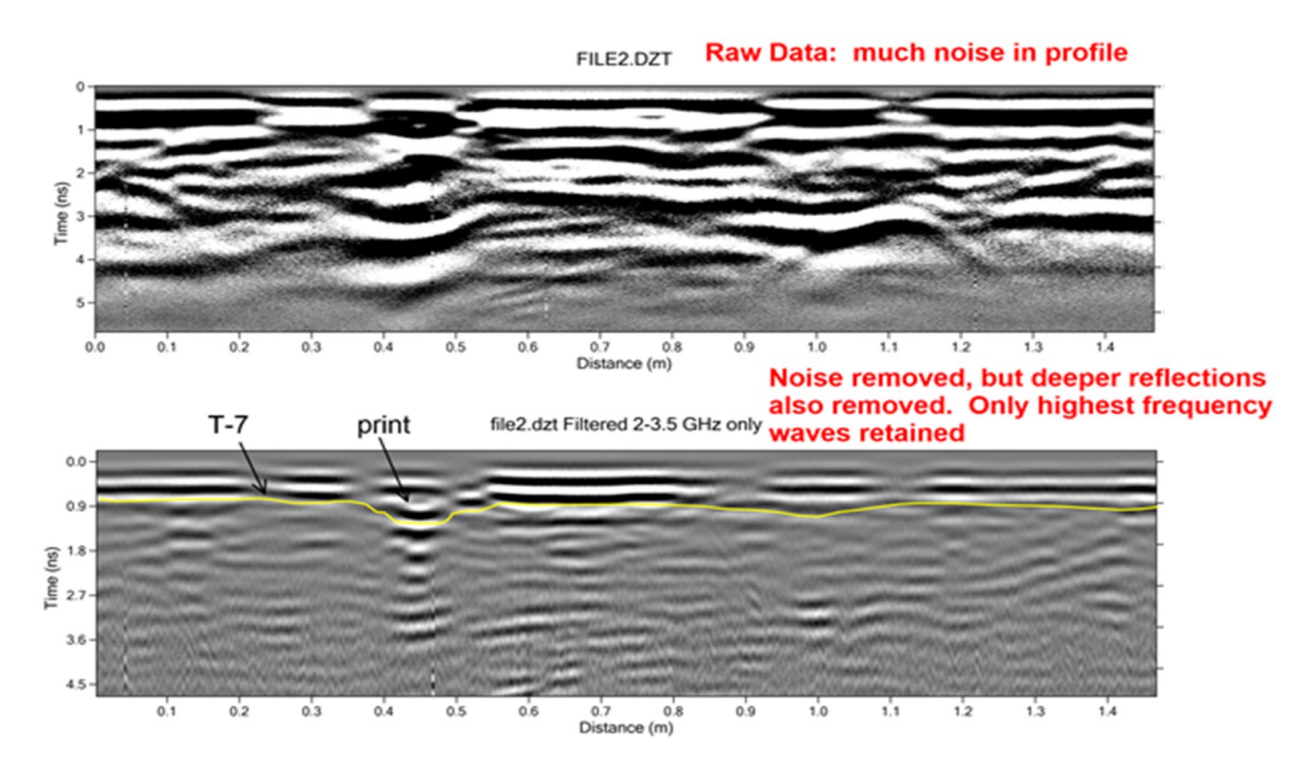


Figure 1: Example of frequency filtering of a 2.6 GHZ profile displaying only the 2-3.5 GHZ reflections that enhance the T-7 reflection and remove noise. These prints are of rhinos from Laetoli Site A.

The two-dimensional profiles in the grid were then interpreted individually with the T-7 identified (as in the yellow horizon shown in Figure 1). The depths of this horizon were compiled into a spreadsheet and contoured using *Surfer* software to produce buried-topography maps and three-dimensional images of the T-7 surface. Often these maps were very "busy" as they contained linear reflection features produced from fractures, roots and amorphous depressions of unknown origin, which were not prints. To remove the "noise" from these images the three-dimensional data were then filtered to remove linear features (cracks), leaving only the depth values of the prints and other depressions on the T-7 surface.

Data collection and processing into 3-D images

A flexible yoga mat was placed on a cleared ground surface to allow maximum energy coupling with the ground and as little void space between the antenna base and the ground surface. The antennas were placed on this mat and moved along strings in 150 cm long linear transects (Figure 2).



Figure 2: Collecting profiles with the 2.6 GHz antenna on a yoga mat, with strings along which the antenna was moved spaced 5 cm apart. A laser in the antenna allowed it to be moved along the strings in a perfectly straight line, with black grid edges showing the start and end of each profile. In this fashion all grids were exactly 150 cm wide and all profiles perfectly straight and separated from each other by 5 cm.

As a model for what prints should look like in profiles, a grid was collected adjacent to where rhinoceros prints were exposed. Very distinct depressions on the T-7 surface were readily visible (Figure 3).

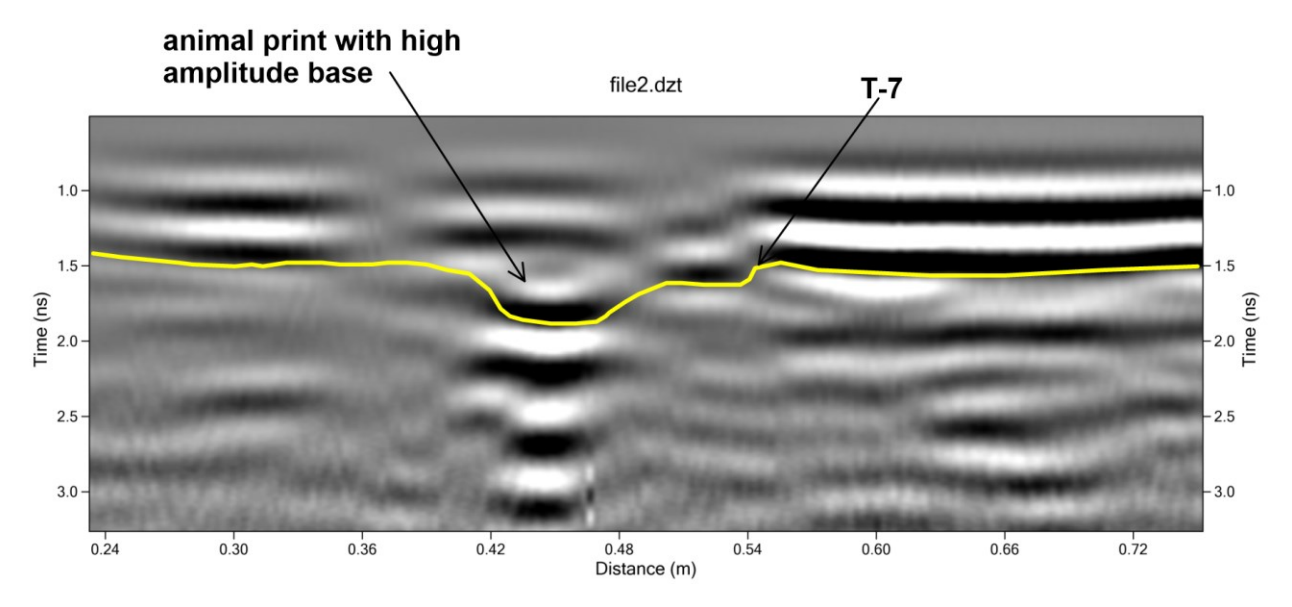


Figure 3: A distinct rhino print on the T-7 surface with a high amplitude reflection at the base of the print. The T-7 surface is very distinct here and not disturbed by fractures or roots.

The readily-visible rhino prints were helpful in interpreting areas of the test grid where fractures had complicated the reflection images. The complexity of the T-7 surface can be readily viewed where

exposed, showing fractures, which are filled with calcite cement and also other depressions of unknown origin (Figure 4).



Figure 4: Fractures, animal burrows and other unknown depressions complicate the T-7 surface.

Reflection profiles that cross fractures, similar to those in Figure 4, are distinctly visible as offsets in the T-7 surface (Figure 5). Depending on the orientation of the fractures and the angle that the GPR profiles cross these features, the profiles can display a variety of complicated reflection features, which are often difficult to interpret.

Another interesting print feature was visible in a small grid collected adjacent to rhinoceroses prints (Figure 6) at Site A. These prints are about 5-6 cm in depth and show distinct lips, where the T-7 sediment was pushed up adjacent to the depression (Figure 6).

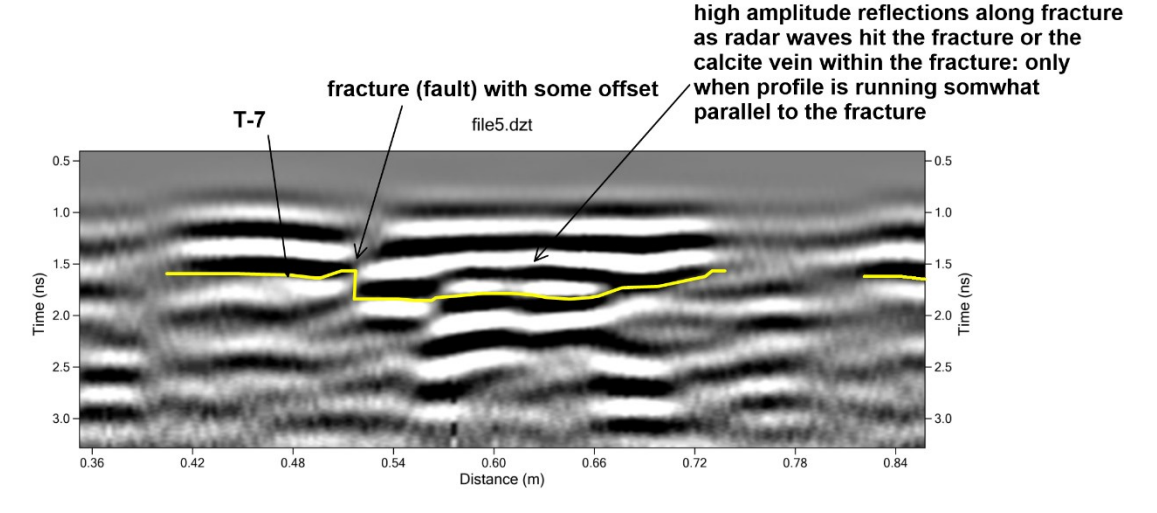


Figure 5: GPR reflection profile that runs approximately parallel to a fracture showing a small offset at a fracture or fault.



Figure 6: Rhino prints (P) trending into the area where a test grid was collected. These prints are wide and relatively deep with lips around the edges where the T-7 mud was pushed up with each step (colloqually known as "squish marks").

The prints show up distinctly in GPR reflection profiles (Figure 7) with both the distinct depression and the adjacent squish marks. There is also a distinctively higher wave amplitude of the T-7 surface at the base of the prints, caused by energy focusing and lower amplitude on the adjacent lips from wave scattering (Conyers 2023: 79).

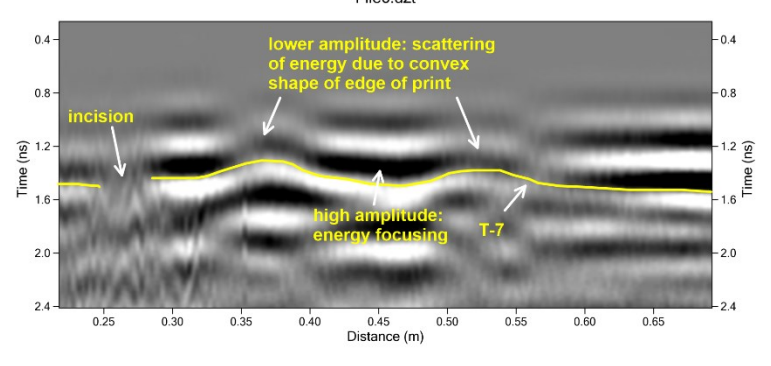


Figure 7: Well developed rhino print depression with focusing or radar energy at its base, and adjacent lips with lower energy due to wave scattering on these squishs marks.

Hominin prints at Site S

A 1.5x12.3-meter grid of GPR reflection profiles were collected at Site S (Figure 8) between the L-8 and M-9 excavations of Masao et al. (2016). Here one trackway of hominid prints was uncovered where the individual can be seen to have been walking from southeast to northwest. The GPR grid was located to "connect the trackway" between the L-8 and M-9 excavations.



Figure 8: Location of GPR grid at Site S.

Each print was mapped individually, and data were processed in the same fashion as the rhino prints, which were used as a model on how to map these depression features. The prints at Site S are equal in complexity to the rhino print model with abundant fractures, roots and other extraneous depressions (Figure 9).



Figure 9: Some of the prints from Site S showing other unknown depressions and abundant fractures of the T-7 surface (from Masao et al. 2016).

Some of the prints at Site S that were uncovered are very well developed (if distorted sometimes by fractures), and exhibit distinct toe, arch and heel features.



Figure 10: Prints in L-8 excavations from Masao et al. (2016) showing toe marks and distinct arch and heels, often cut by fractures filled with calcite.

Each print defined with GPR was identified in all adjacent two-dimensional profiles, and the T-7 surface depth was digitized for 3-D display. Reflection profiles show an abundance of features on the T-7 surface, mostly undulations. When the vertical scale is exaggerated, as in Figure 11, the print can be difficult to differentiate from the numerous other depressions. All were digitized and mapped, and the resulting buried T-7 surface was visualized to differentiate the prints from the abundant other features.

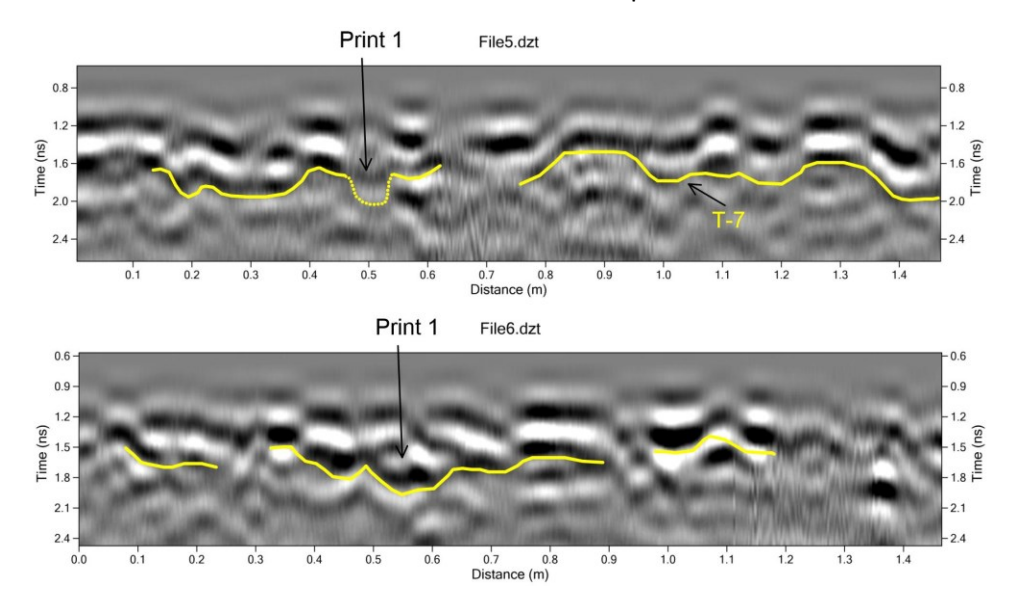


Figure 11: Two adjacent profiles showing Print 1, with its base reflection visible when the print is wider, and invisible when the profile crosses a narrower part of the print.

The resulting buried topographic map of the T-7 surface (Figure 12) was then visualized in a contour map, with the depression areas colored blue. These surface maps could sometimes be very complicated due to the abundance of non-print features. Only when many prints were displayed in one map, and the distance and orientation of them were visualized, could the trackway be defined. Depth data were then processed into a 3-D image to display the variation on the T-7 surface and the distinct print with ball and heel depressions (Figure 13). These surface images were shaded, colored and lit with "artificial sunlight" to enhance the display and differentiate the prints from other features.

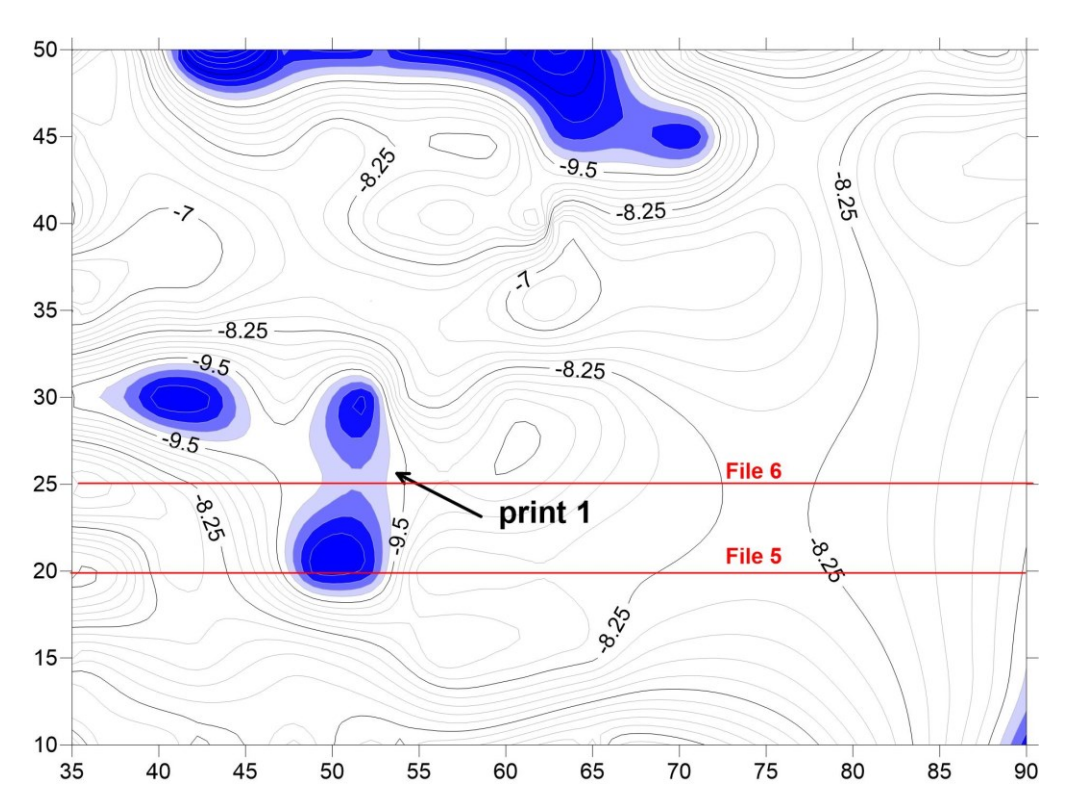


Figure 12: Contour map of Print 1. The location of profiles 5 and 6 shown in Figure 11 are located.

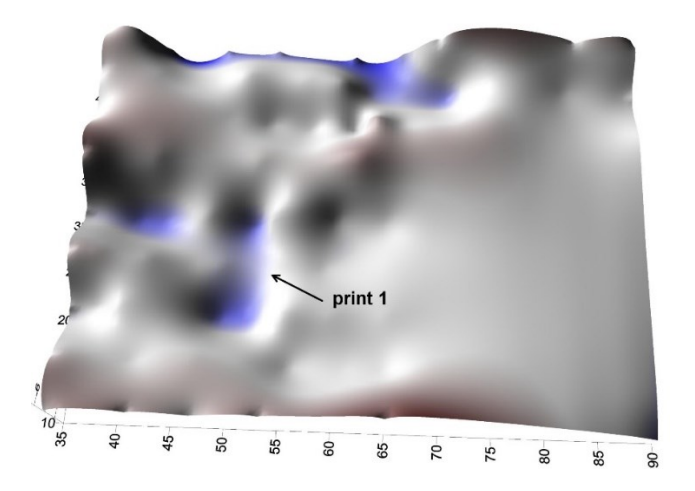


Figure 13: Three-dimensional image of Print 1.

There are a variety of other prints "types" that can be visualized in reflection profiles. They sometimes lack a base, as shown for Print #2 (Figure 14). Here one profile shows the T-7 surface truncated, with no distinct base to the print while an adjacent reflection profile 15 cm away displayed a distinct base. The differences here is related to radar energy attenuation, perhaps due to the material that filled in the print when the site was covered. Perhaps future geochemical analysis can be performed on samples the overlying T-8 tuff unit to determine electrical conductivity variations, which cold explain this phenomenon.

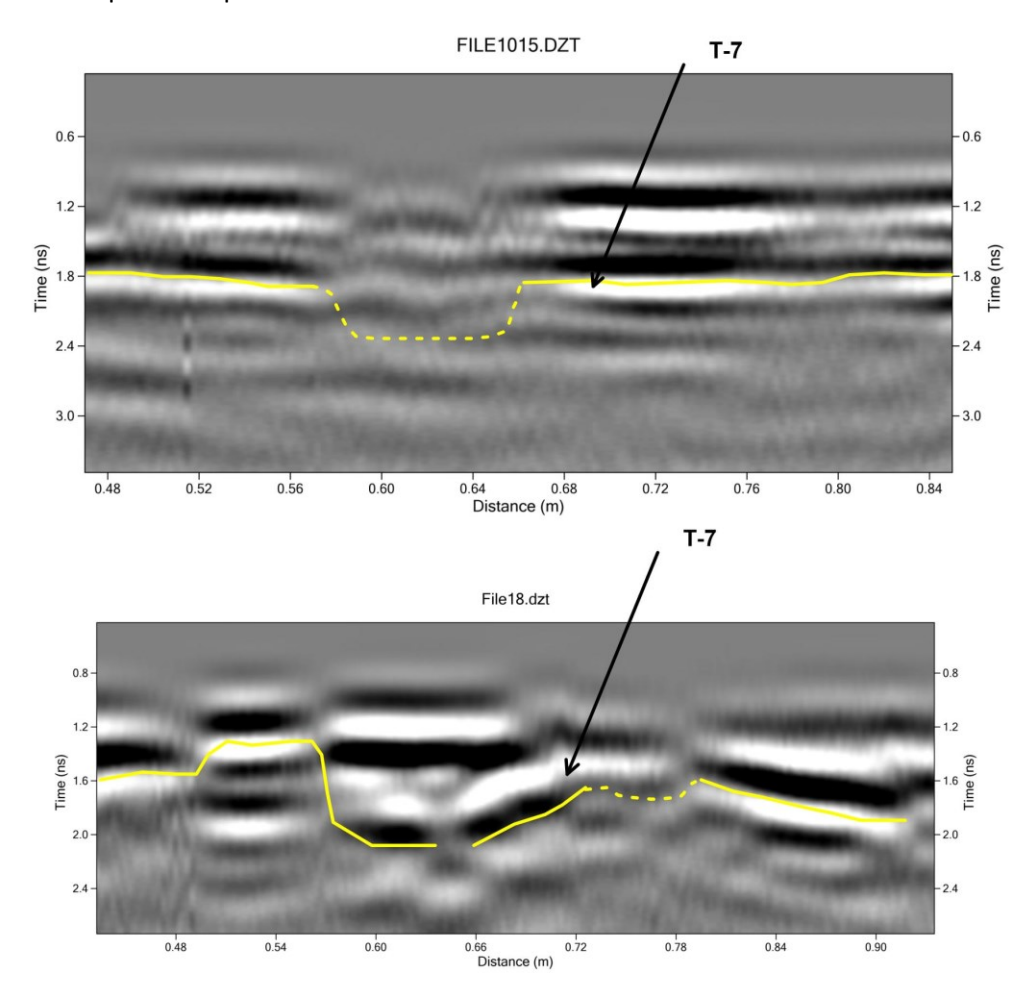


Figure 14: Adjacent reflection profiles separated 15 cm showing different view of Print #2. In the upper reflection profile, the T-7 surface is truncated, and perhaps filled with material that attenuated radar waves. The lower profile shows the distinct base of the print with high amplitude reflections generated from the interface of the T-7 and the print fill sediment.

A contour map of Print #2 shows an elongated print with no distinct ball and heel features (Figure 15). This less-distinct elongated print shape is much like a few of those described by Masao et al. (2016) that display drag marks.

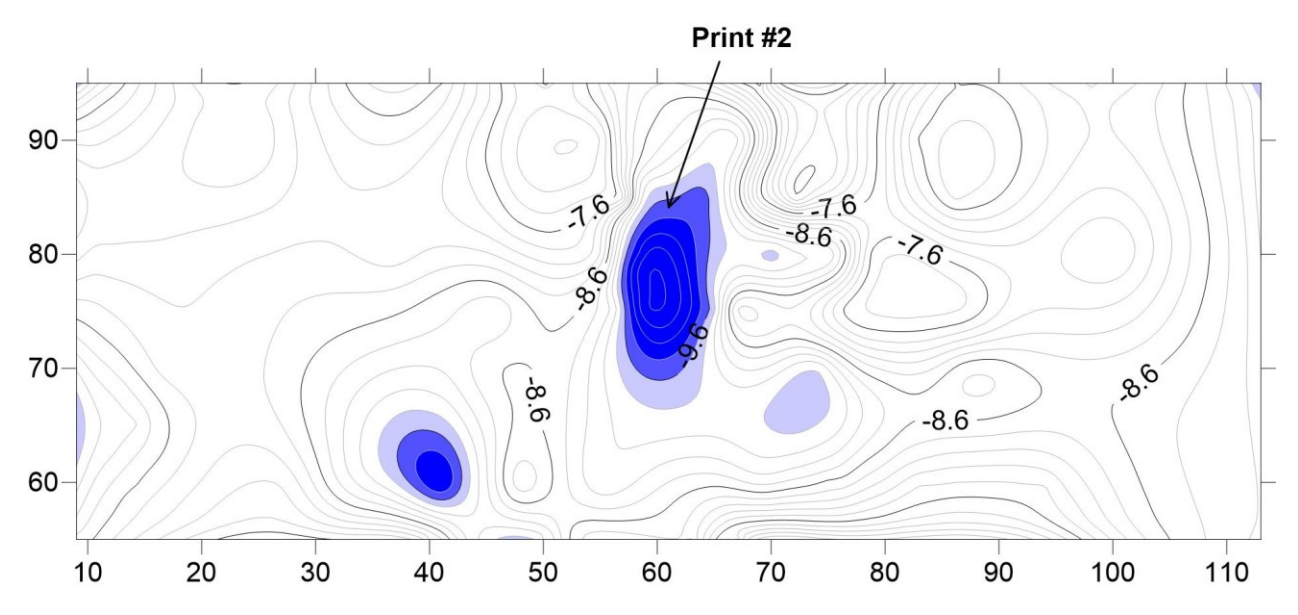


Figure 15: Print #2 contour map showing the elongated depression, likely due to foot drag on the muddy T-7 surface.

A high-resolution contour map produced from data where fractures and miscellaneous other depressions are filtered out shows this drag feature in Print #2 nicely (Figure 16).

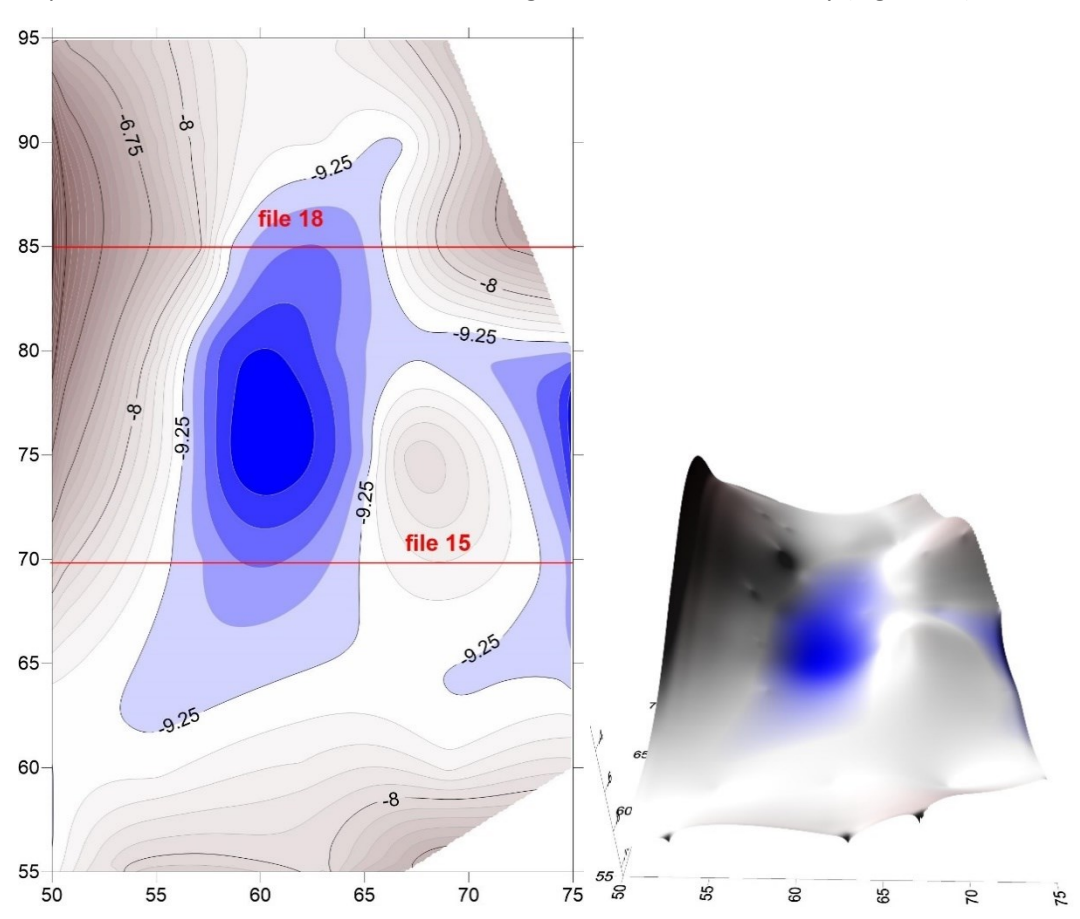


Figure 16: The elongation of Print 2 is visible in this filtered contour map and three-dimensional image.

Analysis of the grid as a whole

There are a wide variety of GPR images that display the prints in the grid between excavations M-9 and L-8 at Site S. This is not surprising, considering the variation in the prints that were exposed in those areas as described by Masao et al. (2016). Most have a few basic aspects in common, which are "double depressions" that are paired ball and heel depressions. These are often distorted in the GPR images due to fractures, roots and possible erosion on the T-7 surface, all of which reflected radar waves in varying ways as they moved back to the surface to be recorded. The average length of prints, as mapped with GPR, is well within the variation measured from the excavations (between 24.5 and 27.3 cm from Masao et al. 2016). The distance between steps as mapped with GPR, was also almost exactly that measured from the nearby excavations by Masao et al. (2016), varying between 50 and 66 cm.

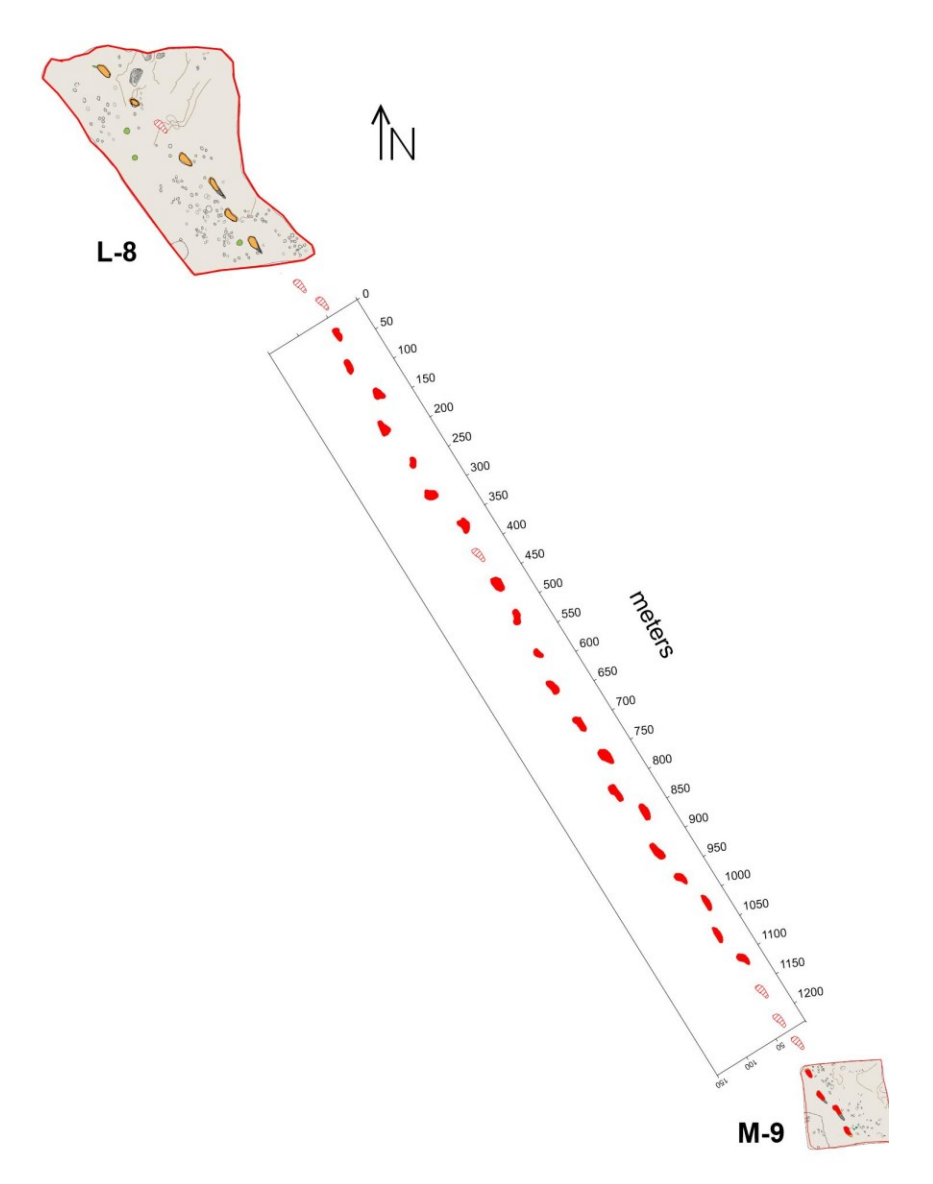


Figure 17: The prints at Site S trackway as defined with GPR and those mapped in excavations L-8 and M-9 by Masao et al. (2016).

The GPR imaged prints are not nearly as distinct as those which were exposed in excavations due to the resolution of the radar waves that were reflected from the T-7 surface. The 2.6 GHz antenna transmits waves of about 3 cm wavelength in this ground, meaning that their minimum vertical resolution is about 1.5 cm (50% of the wavelength: Conyers 2023: 67). When all prints were mapped in space, both from excavations L-8 and M-9 and the GPR-mapped prints, 30 prints can now be defined at Site S. These include 10 that were exposed in the excavations (one remained invisible there due to erosion of the T-7 surface) and 20 with GPR (3 that were invisible probably due to similar subsurface situations), with 3 prints projected in space where there was neither excavations nor GPR mapping.

Artificial intelligence experiments

As an experiment in using artificial intelligence (AI), I created a variety of "models" of what prints look like in reflection profiles. These were then used in an AI analysis by Luca Piroddi and Augusto Montisci (University of Cagliari, Italy) as a first step to determine if these methods could expedite the identification and mapping of prints at Laetoli. Six two-dimensional models that were first digitized (Figure 18). These reflection profiles display prints where the T-7 surface was depressed and truncated, where the base of the prints produced a high amplitude focusing reflection feature, and where there are depressions of the tuff surface, but no focusing or removal of the upper reflection surface. These models were used irrespective of their depth (as measured in time) and served only as image models for AI.

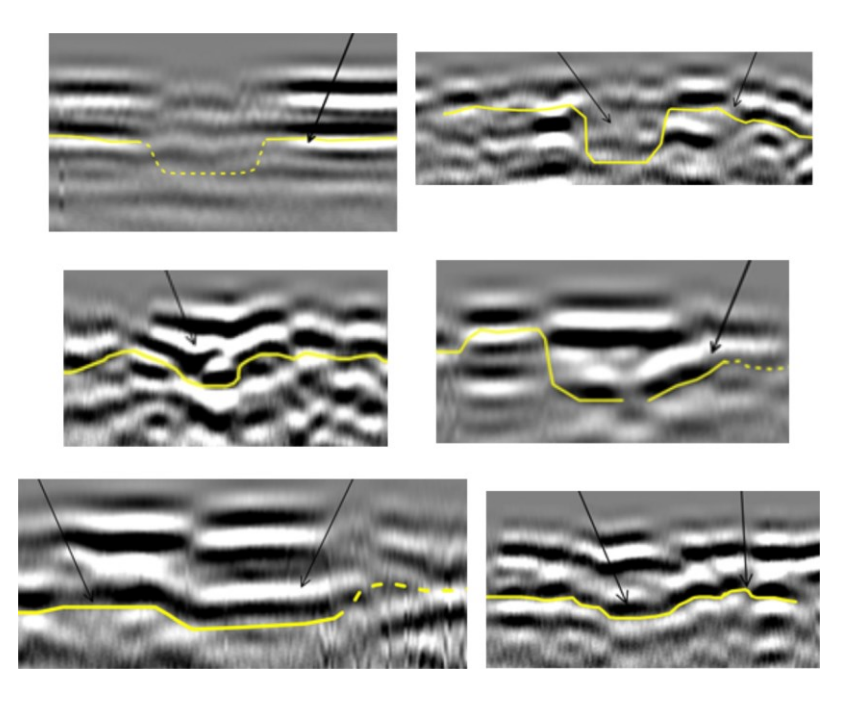


Figure 18: Reflection profile models uses in the AI analysis.

All profiles in a portion of the grid was used as an AI experiment. The reflection profiles were first processed into images and the AI system compared those in Figure 18 to the dataset. When correspondence was made, the portions of the profiles where there was an 95% or greater match were plotted as dark blue (Figure 19). Lesser correspondence was plotted in lighter blue. Print #8, which I could not find in my analysis was also "invisible" in the AI comparative analysis. For the other 11 prints

in this portion of the grid there was a very good general correlation between the GPR mapped prints, and the areas where the AI-generated analysis displayed possible prints. These AI-mapped areas do not display details of the prints but only areas of correspondence to the models. More detailed print geometry was accomplished only with a manual interpretation of the profiles. The AI model was, however, excellent in showing where the likely prints are likely located, but with little detail. Often the AI-analysis defined areas adjacent to the prints where the tuff reflection was visible, but not the area of "no reflection" where the T-7 surface had been depressed and was not resolved with GPR (as in the upper two reflection profiles in the models in Figure 18).

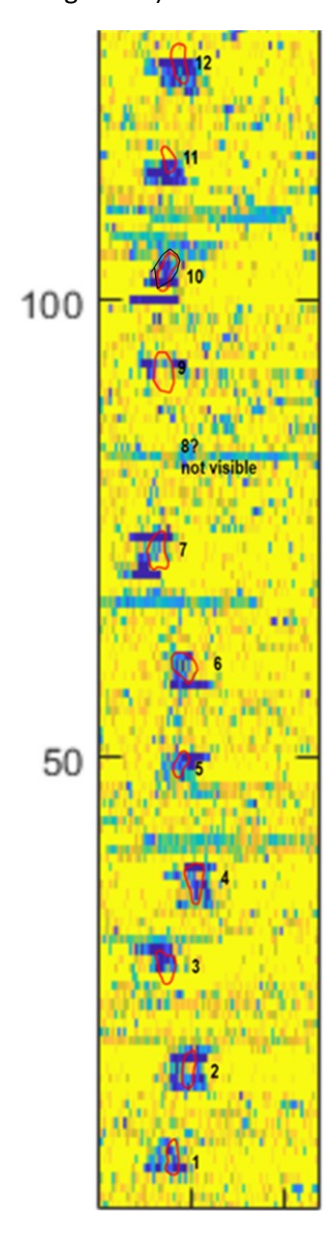


Figure 19: Al generated footprint location compared to the manual interpretation.

This simple AI analysis shows the utility of the method as a "first pass" in interpretation. In the future It can be applied to a much larger grid of reflection profiles to focus on the most likely prints. Their size, location, orientation and distance between the reflection features that correspond to the

models can then be used to interpret the most likely patterns that represent a trackway. A greater refinement of the print models, and a more detailed output of the size and depth of individual prints with AI is also possible. Here the method was utilized only as a preliminary interpretation method for these subtle, but variable, reflection features.

Conclusions

High resolution GPR mapping of the Laetoli prints at Site S was made using the 2.6 GHz antennas. Data needed to be frequency filtered for the prints to be visible. Manual interpretation of the T-7 tuff surface, on which the prints are preserved, produced a variety of print shapes and sizes, which corresponds well to the prints exposed nearby. Fractures and other depressions of unknown origin were filtered out in this process. A total of 20 prints were defined with GPR, and with the other 10 exposed in the nearby excavations, a trackway of 30 prints is now well-defined. Artificial intelligence software was used to identify shapes in 2-D profiles that corresponded to models that had been constructed. This procedure showed a greater than 95% success in using this automated method to discover prints. The AI method was not suitable for producing detailed maps of individual prints, however, and for this the manual interpretation method is still superior.

Acknowledgments

Many thanks to Charles Musiba, Duke University, who is the PI for this research, obtained funding and made arrangements for field work. Funding was supplied by National Geographic Society. Isaac Onoka, University of Dodoma, Tanzania, was instrumental in data collection and analysis at Laetoli.

References

Conyers, Lawrence B. (2023). Ground-penetrating Radar for Archaeology, 4th Edition. Rowman & Littlefield, Lantham, Maryland.

Masao, F.T., Ichumbaki, E.B., Cherin, M., Barili, A., Boschian, G., Iurino, D.A., Menconero, S., Moggi-Cecchi, J. and Manzi, G., (2016). New footprints from Laetoli (Tanzania) provide evidence for marked body size variation in early hominins. Elife, 5, p.e19568.